Water Supply Network Flow Rate Prediction for Short-Duration by STL-LSTM

Yiming Zhang[1a*], Changtao Wang[1b], Xiaoming Han[2c], Yetian Tian[2d] and Xinxin Wang[2e]

[1] School of Control Engineering and Science of Shenyang Jianzhu University, Shenyang 110168, China
[2] Research and Development of Liaoning Dinghan Qihui Electronic System Engineering Co., Ltd, Shenyang 110020, China

[a]zhangyiming@stu.sjzu.edu.cn, [b]wangchangtao@sjzu.edu.cn, [c]hanxiaoming@dinghantech.com, [d]tianyetian@dinghantech.com, [e]wangxinxin@dinghantech.com

Abstract. Accurate prediction of flow in water distribution networks is essential for improving the operational efficiency of urban water supply systems and optimizing resource allocation. To address this need, this paper presents a short-duration flow prediction model for user nodes within a water distribution network. The proposed approach integrates seasonal-trend decomposition (STL) of flow sequences with a long short-duration memory (LSTM) network enhanced by multi-feature inputs. The modeling process begins with linear interpolation to preprocess the flow sequence, ensuring data continuity. The STL method is then employed to decompose the sequence into trend, seasonal, and residual components. Each component is modeled separately using dedicated LSTM networks to capture its unique temporal characteristics. The predicted components are subsequently aggregated to reconstruct the final short-term flow forecast. To evaluate model performance, residual analysis is conducted, confirming the robustness of the proposed approach. Furthermore, comparative experiments are performed against benchmark models including CNN, LSTM, and STL-CNN. Results show that the STL-LSTM model achieves a reduction in forecasting error of over 3% on half-hourly data, and it is verified that STL is not suitable for combining with CNN.

Keywords: Hybrid Models, LSTM, STL Decomposition, Time Series Predition Models, Water Supply Network.

1 Introduction

Accurate short-duration flow forecasting is essential for urban water supply management[1,2]. Existing methods—including statistical models (e.g., ARIMA) [3,4], regression methods[5], and machine learning techniques such as SVM and LSTM[6,7]—face limita-

© The Author(s) 2026
D. Magni et al. (eds.), *Proceedings of the 2026 3rd International Conference on Applied Economics, Management Science and Social Development (AEMSS 2026)*, Advances in Economics, Business and Management Research 389,
https://doi.org/10.2991/978-94-6239-672-2_40

tions in modeling nonlinear, seasonal, and distribution-shift dynamics. Hybrid frameworks integrating time-series decomposition and deep learning have therefore gained attention. STL decomposes series into trend, seasonal, and residual components, enabling component-wise modeling and improved forecasting performance [8-10]. However, most studies focus on hourly or daily horizons, and half-hourly decomposition-based hybrids remain limited. This study proposes an STL-LSTM framework for 30-minute flow prediction, enhancing accuracy and capturing nonlinear temporal dynamics. The main contributions are as follows:

1. Integration of STL decomposition with multi-channel LSTM modeling for component-wise learning.
2. Validation under cross-season distribution shifts (heating and non-heating periods).

The remainder of this paper presents the data and preprocessing, model architecture, experimental evaluation, and concluding discussion.

2 Data Preprocessing

2.1 Data Preparation

Flow data were collected from high-rise and low-rise residential pump nodes in Shenyang, China. Cumulative flow values were recorded at 5min intervals during: March 28 – April 28, 2024 and July 1 – July 31, 2024. The 5min cumulative flow data showed limited variability and were resampled to 30min intervals with linear interpolation to construct the dataset. The series was smoothed to reduce noise, and first-order differencing was applied to obtain the short-duration flow rate Q_i. ($m^3/30\text{min}$), as defined in (1).

$$Q_i(t) = Q_c(t) - Q_c(t-1) \tag{1}$$

Where Q_i is the short-duration flow at t, and Q_c is the cumulative flow at t and $t-1$.

Figures 1 and 2 present high-rise flows exhibit pronounced morning-evening peaks, while low-rise flows display smaller amplitude and longer plateaus, motivating decomposition-based modeling.

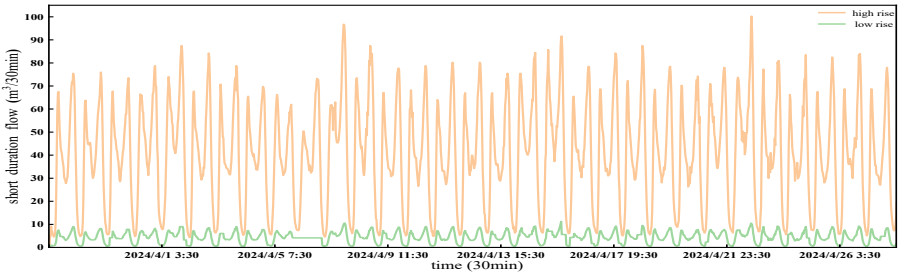

Fig. 1. Half-hourly short-duration flow data, March 28 to April 28, 2024

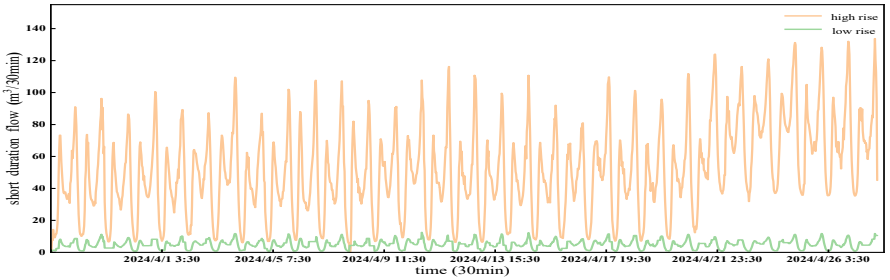

Fig. 2. Half-hourly short-duration flow data, July 1 to July 31, 2024

To validate the assumption of stability in the experimental dataset, it is essential to perform a stationarity test. Stationarity was assessed using the Augmented Dickey-Fuller (ADF) test at a 0.05 significance level. All datasets rejected the null hypothesis of unit root, indicating stationarity after preprocessing. Thus, the data satisfy modeling assumptions.

3 STL-LSTM Model Construction

3.1 STL Decomposition

Seasonal-Trend decomposition using LOESS (STL) decomposes a time series Y_t into seasonal S_t, trend T_t and residual R_t components using locally weighted regression. The method employs iterative inner and outer loops for component extraction and robustness weighting to mitigate outliers. The overall procedure is illustrated in Figure 3.

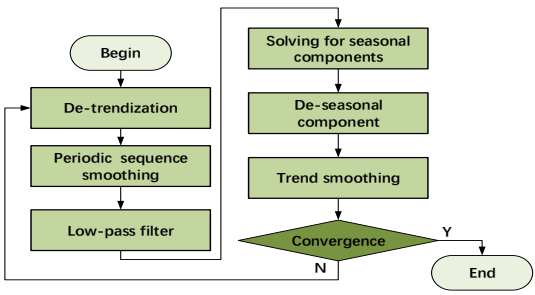

Fig. 3. STL decomposition of the inner loop process

3.2 Multi-Channel LSTM Model

Long Short-Term Memory (LSTM) is a deep learning architecture widely used in time series forecasting and sequence modeling. Unlike conventional neural networks, the basic unit of the LSTM hidden layer is the memory block, as shown in Figure 4.

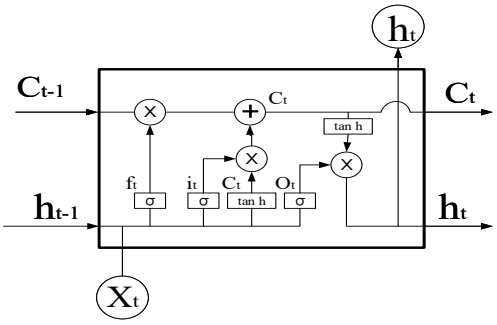

Fig. 4. Memory block

In the figure σ is the Sigmoid function; h_{t-1} is the output of the previous cell; x_t is the input;C_t is the cell state; f_t is the forget gate; i_t is the input gate; Q_t is the output gate.

The forget gate scales the previous cell state using sigmoid-activated weights derived from the current input and hidden state. The input gate generates sigmoid weights and a tanh candidate state, whose element-wise product updates the cell state. The output gate applies sigmoid weights to the tanh-transformed cell state to produce the final output and next hidden state In (2)–(4), W_x and b_x denote the corresponding weights and biases; the state update from $C_{t-1} \to C_t$ process is as in (5)-(7).

$$f_t = \sigma\left(W_f \times [h_{t-1}, x_t] + b_f\right) \tag{2}$$

$$i_t = \sigma\left(W_i \times [h_{t-1}, x_t] + b_i\right) \tag{3}$$

$$O_t = \sigma\left(W_o \times [h_{t-1}, x_t] + b_o\right) \tag{4}$$

$$C_{0t} = \tanh(W_C \times [h_{t-1}, x_t] + b_C) \tag{5}$$

$$C_t = f_t \times C_{t-1} + i_t \times C_{0t} \tag{6}$$

$$h_t = O_t \times \tanh(C_t) \tag{7}$$

Then perform hyperparameter tuning. Two datasets are split 8:2 into training and test sets. The study minimizing MAPE by adjusting the number of hidden units and training epochs. MAPE is defined in (8), where y_i is the actual value, y_{pi} is the prediction, and n the number of forecasts. The corresponding errors are summarized in Table 1.

$$MAPE(\%) = \frac{1}{n}\sum_{i=1}^{n}\left|\frac{y_i - y_{pi}}{y_i}\right| \times 100\% \tag{8}$$

Table 1. Mape for LSTM

Hidden Units	Epochs	MAPE_High	MAPE_Low
100	700	14.57%	20.87%
100	1000	12.36%	15.12%
300	700	10.28%	12.48%
300	1000	7.57%	8.81%

Optimal performance was obtained with 300 hidden units and 1,000 epochs using the Adam optimizer (learning rate 0.0005). These settings were adopted for the hybrid model. Error metrics indicate that the standalone LSTM achieved limited predictive accuracy.

3.3 STL-LSTM Hybrid Model

The STL-LSTM model uses three LSTM networks trained on the first 80% of the decomposed sequences S_t, T_t, and R_t with the remaining 20% for testing. Hyperparameters follow the configuration defined previously. The predicted components S_{pt}, T_{pt}, and R_{pt} are obtained using step size $n$for feature construction, then inverse-normalized to yield S_{pt}, T_{pt}, and R_{pt}, which are combined as:

$$Y_p = S_p + T_p + R_p \tag{9}$$

Where Y_p is the final predicted short-duration flow.

4 Experiments and Results

Figure 5 and 6 present the prediction results of short-duration flow data from the STL-LSTM model test set for the periods March 28 to April 28 and July 1 to July 31, 2024, respectively.

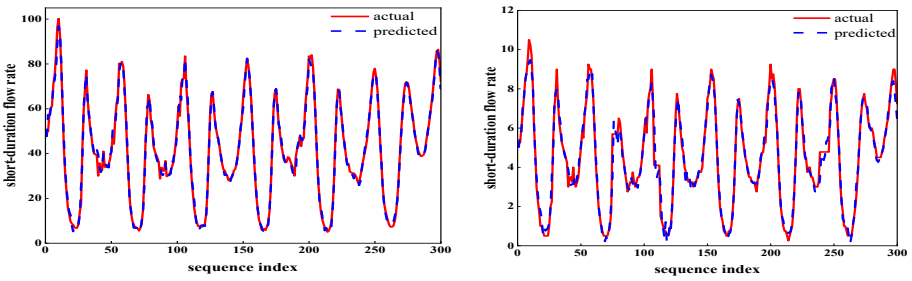

(a) Predicted results for high-rise short-duration flows (b) Predicted results of low-rise short-duration flows

Fig. 5. 03.28-04.28 short-duration flow prediction results

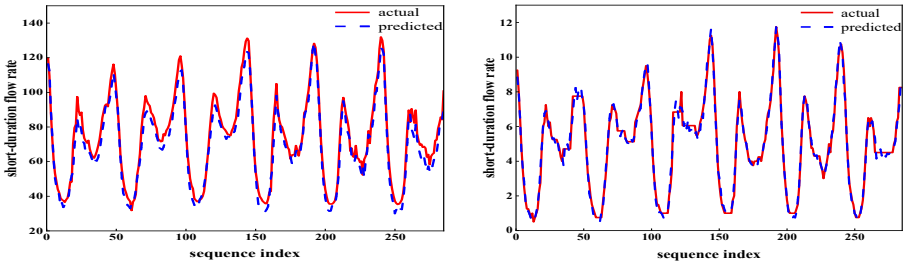

(a) Predicted results of high-rise short-duration flows (b) Predicted results of low-rise short-duration flows

Fig. 6. 07.01-07.31 short-duration flow prediction results

All of the above experimental results are based on the premise that the residual sequences passed the Ljung-Box test, confirming that there is no significant autocorrelation in the residuals and thereby validating the effectiveness of the model.

During the model evaluation phase, comprehensive performance assessment was conducted using metrics such as Root Mean Square Error (RMSE) and MAPE. This ensures the practical use of the model. The RMSE formula is as follows:

$$RMSE = \sqrt{\frac{1}{n}\sum_{i=1}^{n}(y_i - y_{pt})^2} \tag{10}$$

The meanings of the variables are consistent with (8). Smaller values of MAPE and RMSE indicate higher model accuracy.

After hyperparameter tuning, all models reached optimal configurations; however, STL-CNN exhibited substantially higher prediction errors than CNN, LSTM, and STL-LSTM, as shown in Table 2. and was therefore excluded from the July 2024 evaluation. Its underperformance stems from limited multi-channel feature extraction after STL decomposition and the inability of CNN to capture long-term temporal dependencies.

Figure 7 and 8 presents a comparison of prediction errors among CNN, LSTM, and STL-LSTM based on short-duration flow data from March 28 to April 28, 2024. In the Figures displays the MAPE values and RMSE values.

Table 2. Mape of training sets for different prediction models

	CNN	LSTM	STL-LSTM	STL-CNN
MAPE_High	3.46%	4.19%	2.06%	18.11%
MAPE_Low	6.08%	7.45%	5.98%	13.50%
RMSE_High	0.044	0.069	0.020	1.193
RMSE_Low	0.050	0.101	0.006	0.127

MAPE and RMSE results indicate that hybrid models outperform single models, with STL-LSTM maintaining high accuracy under noisy conditions. For 30min flow forecasting, STL-LSTM achieves superior precision and generalization. Prediction accuracy is lower for low-rise flow due to smaller magnitude and reduced variability;

after STL decomposition, minor disturbances are amplified, slightly degrading performance relative to high-rise flow.

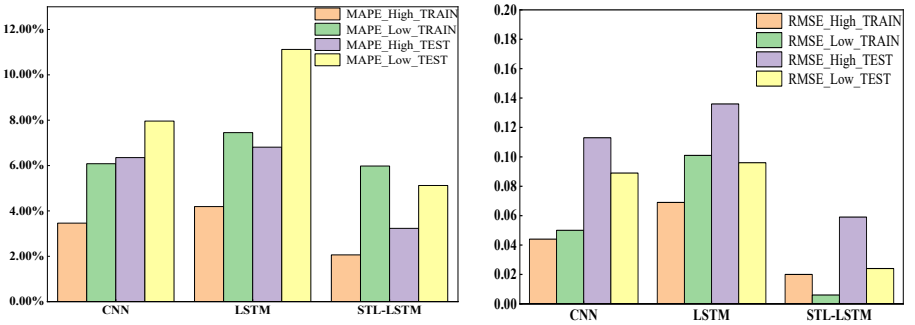

(a) CNN, LSTM and STL-LSTM MAPE comparison (b) CNN, LSTM and STL-LSTM RMSE comparison

Fig. 7. 03.28-04.28 short-duration flow errors

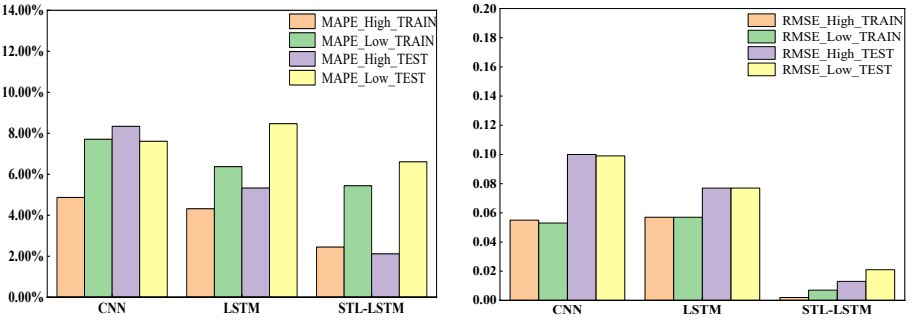

(a) CNN, LSTM and STL-LSTM MAPE comparison (b) CNN, LSTM and STL-LSTM RMSE comparison

Fig. 8. 07.01-07.31 short-duration flow errors

5 Conclusion

This study proposes an STL-LSTM hybrid framework for half-hourly water-flow prediction. By decomposing the series into trend, seasonal, and residual components and modeling them with multi-channel LSTM networks, the approach improves forecasting accuracy and robustness under seasonal distribution shifts.

Compared with CNN and standalone LSTM, STL-LSTM reduces MAPE by over 3% on test datasets. The framework demonstrates strong adaptability and interpretability, making it suitable for intelligent water-supply systems.

Future work will expand validation to multi-city and multi-climate environments and incorporate exogenous variables such as temperature and holidays to enhance generalization.

References

1. Que, Q., Gao, J., Qian, Y. (2024). Water demand forecasting in multiple district metered areas based on a multi-scale correction module neural network architecture. Water Research X, 25, 100269. 10.1016/j.wroa.2024.100269.
2. Mahmood, O. A., Sulaiman, S. O., Al-Jumeily, D. (2024). Forecasting for Haditha reservoir inflow in the West of Iraq using Support Vector Machine (SVM). PLoS One, 19(9), e0308266. 10.1371/journal.pone.0308266
3. Gong X, Li B, Yang Y, Li M, Li T, Zhang B, Zheng L, Duan H, Liu P, Hu X, Xiang X, (2025). Construction and application of optimized model for mine water inflow prediction based on neural network and ARIMA model. Scientific Reports, 15(1), 2009. 10.1038/s41598-025-85477-2
4. Muñoz-Rodríguez, D., González-Ortega, M. J., Aguilera-Ureña, M. J., Ortega-Ballesteros, A., Perea-Moreno, A. J. (2025). Innovation ARIMA models application to predict pressure variations in water supply networks with open-loop control. Case study in Noja (Cantabria, Spain). Energy Nexus, 100423. 10.1016/j.nexus.2025.100423.
5. Sareminia, S. (2023). A support vector based hybrid forecasting model for chaotic time series: spare part consumption prediction. Neural processing letters, 55(3), 2825-2841. 10.1007/s11063-022-10986-4.
6. Zhang Y, Li J, Sun S, Li G, Yang Q, Sun Y, Wang X, Xu C. (2024). Short-Term Water Supply Forecasting for Water Treatment Plant Using Temporal Multi-Scale Features. Water, 16(24), 3573. 10.3390/w16243573.
7. Xu, Z., Ying, Z., Li, Y., He, B., Chen, Y. (2020). Pressure prediction and abnormal working conditions detection of water supply network based on LSTM. Water Supply, 20(3), 963-974. 10.2166/ws.2020.013.
8. Xu, L., Ou, Y., Cai, J., Wang, J., Fu, Y., Bian, X. (2023). Offshore wind speed assessment with statistical and attention-based neural network methods based on STL decomposition. Renewable Energy, 216, 119097. 10.1016/j.renene.2023.119097.
9. Jaiswal, R., Jha, G. K., Kumar, R. R., & Choudhary, K. (2025). STL-LSTM Hybrid Model for Forecasting Seasonal Agricultural Price Series. Annals of Data Science, 1-24. 10.1007/s40745-025-00590-3
10. Lazcano de Rojas, A., Jaramillo Morán, M. Á. (2025). Data preprocessing techniques and neural networks for trended time series forecasting. 10.1016/j.asoc.2025.113063.

Open Access This chapter is licensed under the terms of the Creative Commons Attribution-NonCommercial 4.0 International License (http://creativecommons.org/licenses/by-nc/4.0/), which permits any noncommercial use, sharing, adaptation, distribution and reproduction in any medium or format, as long as you give appropriate credit to the original author(s) and the source, provide a link to the Creative Commons license and indicate if changes were made.

The images or other third party material in this chapter are included in the chapter's Creative Commons license, unless indicated otherwise in a credit line to the material. If material is not included in the chapter's Creative Commons license and your intended use is not permitted by statutory regulation or exceeds the permitted use, you will need to obtain permission directly from the copyright holder.